PNAS
www.pnas.org

Supplementary Information for

The Great Oxidation Event preceded a Paleoproterozoic snowball Earth

Matthew R. Warke, Tommaso Di Rocco, Aubrey L. Zerkle, Aivo Lepland, Anthony R. Prave, Adam P. Martin, Yuichiro Ueno, Daniel J. Condon and Mark W. Claire

Corresponding author name: Matthew Warke
Email: mw438@st-andrews.ac.uk

This PDF file includes:

Supplementary text
Figures S1 to S2
Tables S1 to S3
Legend for Datasets S1
SI References

Other supplementary materials for this manuscript include the following:

Dataset S1

Supplementary Information Text

Methods

Core sampling of FAR-DEEP cores 1A and 3A was conducted at the core repository at the Geological Survey of Norway, and all samples were assigned an International Geo Sample Number (IGSN) in-line with sampling procedures (1). Core samples were cut perpendicular to bedding and a portion of the core was crushed and milled to a fine powder using an agate ball mill. The two-step sequential extraction of acid volatile sulfur (AVS) and then chrome reducible sulfur (CRS) phases was achieved by first refluxing the sample with 6 M HCl followed by (when the reaction is complete) refluxing with acidified 1M $CrCl_2$ (2–4). Evolved sulfide was captured using a 1 M $AgNO_3$ solution to form Ag_2S.

For $\delta^{34}S$ analysis Ag_2S samples were placed in tin capsules and loaded into a Costech Zero Blank autosampler and then dropped into a 1020 °C reactor tube where they combusted in the presence of O_2. Combustion products were carried by helium stream through tungstic oxide combustion catalysts and copper wire was used as a reductant for any excess O_2. Water was removed by using a magnesium perchlorate trap at room temperature before entering a GC column for gas separation. A Thermo ConFlo IV allowed connection between Thermo Isolink Elemental Analyser and MAT 253 IRMS by an open split interface, which ensures constant pressure in the source. The resulting SO_2 gas was measured in continuous flow mode at the University of St Andrews, Scotland, (*Methodology*) and analytical uncertainty for $\delta^{34}S$ was better than 0.3 ‰ (1σ).

Measured isotopic compositions were calibrated to CDT scale by bracketing Ag_2S samples with international reference standards (IAEA-S2, IAEA-S3). Results are expressed in standard delta notation relative to Vienna Canyon Diablo Troilite (VCDT) (5):

$$\delta^{3X}S = 1000 * [\left(\frac{^{3X}S}{^{32}S}\right)_{\text{sample}} / \left(\frac{^{3X}S}{^{32}S}\right)_{\text{V-CDT}} - 1) \quad (1)$$

where X can equal 3, 4, or 6 depending on the isotope being analysed.

For $\delta^{33}S$ and $\delta^{36}S$ analysis (and calculation of $\Delta^{33}S$ and $\Delta^{36}S$ values), approximately 0.4-0.5 mg of Ag_2S and ~40-50 mg CoF_3 was weighed into an iron-nickel-cobalt alloy foil (pyrofoil) in ~1:100 ratio and the pyrofoil was tightly folded, sealed and placed in a glass reaction tube. Approximately 1 g of NaF crystals were added to the tube in order to consume HF and produce $NaHF_2$. The reaction tube was attached to a vacuum line and placed within a JHP-22 Curie-point pyrolyzer (CPP) (JAI, Japan). The CPP employs induction heating to rapidly heat the pyrofoil which loses its ferromagnetic property at 590°C (6). The glass reactor was pumped down to ~3 $x10^{-3}$ mbar and the position of the pyrofoil was carefully matched to the center of the induction coil to ensure efficient reaction. In an update of ref (6), we performed three pyrolysis reactions per sample, maintaining temperature for 99 seconds, for a total of 297 s of reaction time. This increases total SF_6 yields from ~20-30 % to 40-70 %, thus reducing the Ag_2S sample size needed.

The SF_6 was separated from other gas phases produced in the fluorination reaction (e.g., O_2, HF, CO) by passing the gases through a series of cryogenic freezing steps using both liquid N_2 (-196 °C) and a liquid N_2-ethanol slurry (-95 °C) in a procedure similar to that described previously (Ueno et al., 2015). SF_6 was then passed through a SRI 8610C gas chromatograph to ensure complete separation from other products. The GC is equipped with a 12 ft HayeSep Q packed column (1/8″ OD, 80–100 mesh) and a 12 ft Molecular Sieves 5A packed column (1/8″ OD, 60–80 mesh) operating at a He flow rate of 24 ml/min and at a temperature of 80 ˚C (Ono et al., 2006). SF_6 gas elutes after approximately 26 minutes and is detected by a thermal conductivity detector (TCD). Purified SF_6 was frozen in a glass Hungate tube at liquid N_2 temperature and transferred to the MAT253 microvolume inlet (packed with ~20 1 mm stainless-steel ball bearings in order to increase

total gas pressure) and then expanded into the mass spectrometer source at room temperature. The MAT253 dedicated for minor sulfur isotope measurements is equipped with four Faraday cups with $3x10^8$, $3 x10^{10}$, 10^{10} and 10^{12} Ω feedback resistors for simultaneous measurement of m/z 127, 128, 129 and 131. Sample gas was analyzed and compared to reference SF_6 gas after adjusting the reference bellow volume to obtain equal signal intensity, normally between 3.5 and 5.5 V on m/z 127, for both sample and reference side.

Variations in sulfur isotope ratios are expressed in the δ notation (equation 1) relative to VCDT (5). For mass dependent processes $\delta^{33}S \approx 0.515 \times \delta^{34}S$, and $\delta^{36}S \approx 1.90 \times \delta^{34}S$ (7). Deviations from these predicted quadruple sulfur isotope relationships are expressed using $\Delta^{33}S$ and $\Delta^{36}S$ notation, where:

$$\Delta^{33}S = 1000 * \left[\ln\left(\frac{\delta^{33}S}{1000} + 1\right) - 0.515 * \ln\left(\frac{\delta^{34}S}{1000} + 1\right)\right] \quad (2)$$

$$\Delta^{36}S = 1000 * \left[\ln\left(\frac{\delta^{36}S}{1000} + 1\right) - 1.9 * \ln\left(\frac{\delta^{34}S}{1000} + 1\right)\right] \quad (3)$$

Longer term analytical uncertainty is calculated from 64 measurements of IAEA-S1 conducted over 10 months. IAEA-S1 $\Delta^{33}S$ and $\Delta^{36}S$ values were 0.116 ± 0.015 ‰ and -0.572 ± 0.177 ‰ (mean ± 1σ), respectively (Dataset S1) and are within uncertainty of values reported in other studies (6, 8–10). The long term 1σ standard error serves as a minimum error magnitude on each datapoint. The precision of a single measurement is typically in the range of 0.010 ‰ for $\delta^{33}S$ and $\delta^{34}S$ and 0.100 ‰ for $\delta^{36}S$ determined from IAEA-S1.

Linear regression is a common methodology for determining the $\Delta^{36}S/\Delta^{33}S$ slope of a series of data points on a scatter plot but has some limitations. Linear regression only considers errors in the vertical coordinate when determining the best fit slope and therefore does not produce a meaningful estimate of the uncertainty of the slope. When discussing $\Delta^{36}S/\Delta^{33}S$ slopes we use linear regression for comparison with previous studies, but also discuss results using orthogonal data regression (ODR). This technique incorporates errors in both the abscissa and ordinate and quantifies the uncertainty in the determination of the resulting slope, which can be quite large for small magnitude data.

Computations were carried out using the `odr` module from the *scipy* package within python 3.7.6. We assert that ODR allows for expanded interpretation compared to previous work in the field utilizing linear regression, but users must exert some care in some situations. In particular, the method is known to overpredict slopes if the underlying data is not linearly related (11) as the data in Fig 2C may not be. More broadly, there is no *a priori* reason to consider that true relationship between $\Delta^{36}S$ and $\Delta^{33}S$ is linear. Indeed, (mass-dependent) mass-conservation effects are known to cause a non-linear relationship between these variables (12), so use of ODR for prediction of slope (and associated error) in MDF data sets may be susceptible to enhanced 'equation error' (11).

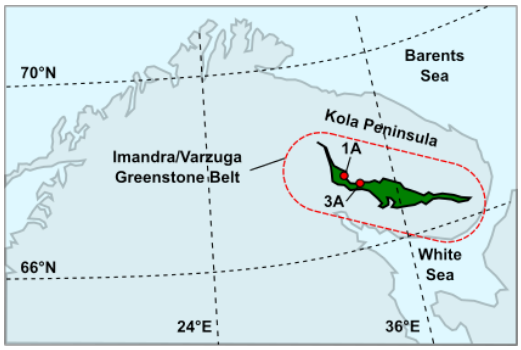

Fig. S1. Regional map showing the location of the Imandra/Varzuga Greenstone Belt on the Kola Peninsula (NW Russian Federation) and the position of FAR-DEEP drillcores 1A and 3A; modified after (13)**.**

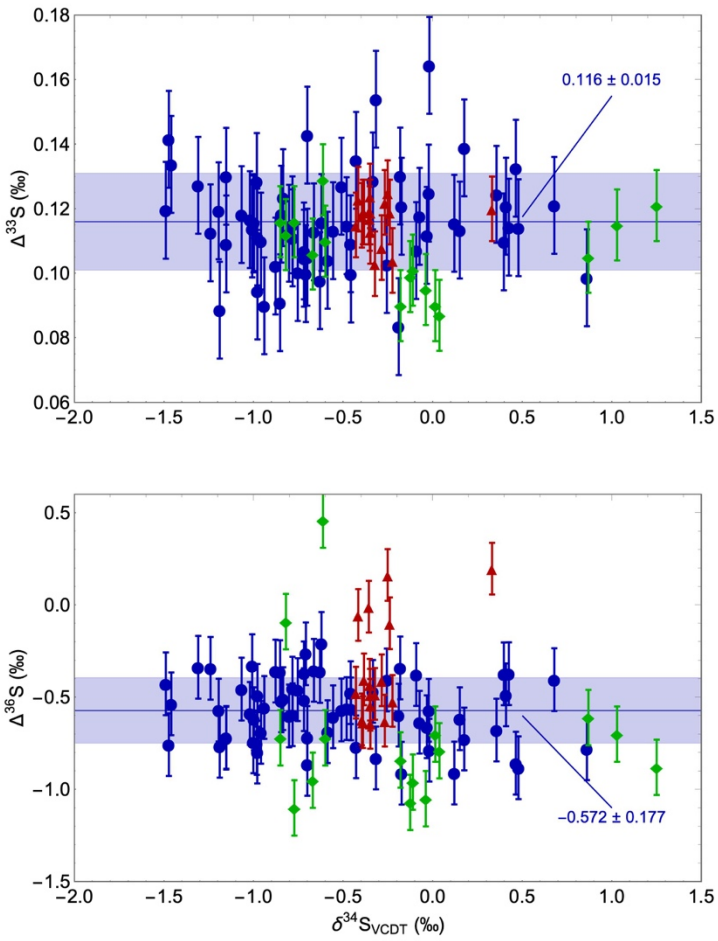

Fig. S2. $\Delta^{33}S$ and $\delta^{34}S$ values (upper panel) and $\Delta^{36}S$ and $\delta^{34}S$ values (lower panel) of IAEA-S1. Blue circles represent data from the University of St Andrews (this study; Dataset S1). Green diamonds and red triangles represent IAEA-S1 data from refs (6) **and** (10)**, respectively. Horizontal blue line shows the mean IAEA-S1 value measured at St Andrews; shaded blue areas represent a 1σ envelope around the mean.**

Table S1. sample metadata and quadruple sulfur isotope data from the Seidorechka Sedimentary Formation (n=24); 'err' signifies a 1σ error

Sample	Rock type	Member	Depth	$\Delta^{33}S$	$\Delta^{36}S$	$\Delta^{33}S$ err	$\Delta^{36}S$ err	$\delta^{34}S$	$\delta^{34}S$ err
LOK003116224	Siltstone	Shale member	71.76	-0.182	-0.330	0.018	0.198	-7.5	0.3
REQ003117152	Siltstone-shale	Shale member	73.91	-0.291	0.553	0.020	0.198	-8.1	0.3
PML3111706_1	Siltstone	Shale member	85.93	-0.071	-0.496	0.025	0.198	-6.4	0.3
LOK003116232	Shale	Shale member	89.83	-0.034	-0.259	0.025	0.264	-4.6	0.3
PML3100540_1	Siltstone-shale	Shale member	95.62	-0.161	0.149	0.018	0.198	-9.1	0.3
LOK003116264	Siltstone	Shale member	108.08	-0.102	-0.143	0.018	0.198	-8.6	0.3
LOK003116268	Shale	Shale member	110.69	-0.057	0.417	0.018	0.198	-8.2	0.3
LOK003116270	Shale	Shale member	111.88	-0.231	-0.066	0.018	0.198	-4.7	0.3
LOK003116276	Siltstone-shale	Limestone-shale member	121.68	0.033	-0.315	0.018	0.198	-0.6	0.3
LOK003116278	Siltstone-shale	Limestone-shale member	123.03	-0.013	0.009	0.020	0.198	-0.2	0.3
LOK003116286	Limestone-shale	Limestone-shale member	129.25	0.251	-0.365	0.029	0.198	-2.2	0.3
LOK003116292	Limestone-shale	Limestone-shale member	133.76	-0.116	0.154	0.018	0.198	1.6	0.3
LOK003116298	Shale	Limestone-shale member	138.73	-0.018	-0.613	0.018	0.198	-5.6	0.3
REQ003117120	Siltstone-shale	Limestone-shale member	141.4	-0.190	0.245	0.019	0.198	-7.6	0.3
LOK003116374	Shale	Limestone-shale member	142.81	-0.181	0.690	0.020	0.198	-7.8	0.3
LOK003116378	Siltstone-shale	Quartzite member	147	-0.362	0.172	0.023	0.198	-8.5	0.3
LOK003116380	Shale-sandstone	Quartzite member	147.81	-0.294	0.567	0.018	0.198	-6.6	0.3
REQ003117124	Siltstone	Quartzite member	155.32	-0.336	0.199	0.018	0.198		
REQ003117126	Sandstone	Quartzite member	156.49	-0.425	1.058	0.018	0.198	-9.4	0.3
LOK003116382	Siltstone	Sandstone-siltstone member	163.37	-0.163	0.397	0.018	0.198	-9.4	0.3
LOK003116384	Shale	Sandstone-siltstone member	167.65	-0.152	0.069	0.018	0.233	-7.0	0.3
LOK003116390	Shale	Sandstone-siltstone member	173.33	-0.084	0.355	0.018	0.198	-10.3	0.3
LOK003116392	Shale	Sandstone-siltstone member	177.61	-0.063	0.017	0.031	0.198	-10.9	0.3
REQ003117136	Shale	Sandstone-siltstone member	186.53	-0.197	-0.079	0.018	0.198	-14.6	0.3

Table S2. sample metadata and quadruple sulfur isotope data from the Polisarka Sedimentary Formation (n=23); 'err' signifies a 1σ error

Sample	Rock type	Member	Depth	$\Delta^{33}S$	$\Delta^{36}S$	$\Delta^{33}S$ err	$\Delta^{36}S$ err	$\delta^{34}S$	$\delta^{34}S$ err
REQ003117014	Shale	Greywacke-Diamictite Member	99.32	0.083	-0.419	0.025	0.198	-0.8	0.3
REQ003117022	Diamictite	Greywacke-Diamictite Member	102.42	-0.004	-0.623	0.018	0.198	0.0	0.3
REQ003117024	Diamictite	Greywacke-Diamictite Member	104.67	0.010	-0.387	0.018	0.198	-0.8	0.3
REQ003117032	Diamictite	Greywacke-Diamictite Member	109.64	0.002	-0.493	0.018	0.198	-0.4	0.3
REQ003117036	Diamictite	Greywacke-Diamictite Member	111.23	0.075	-1.055	0.018	0.198	-0.4	0.3
REQ003117046	Greywacke	Greywacke-Diamictite Member	115.56	0.021	-0.951	0.018	0.198	-1.6	0.3
REQ003117054	Greywacke	Greywacke-Diamictite Member	119.53	0.028	0.739	0.024	0.198	-3.9	0.3
REQ003117056	Greywacke	Greywacke-Diamictite Member	121.25	0.022	-0.202	0.018	0.198	-4.0	0.3
REQ003117060	Dolarenite	Limestone Member	124.37	-0.378	0.545	0.018	0.198	-8.5	0.3
REQ003117066	Shale*	Limestone Member	174.63	0.029	0.343	0.018	0.198	-11.5	0.3
REQ003117074	Calcarenite	Limestone Member	181.44	0.042	0.376	0.018	0.198	-12.0	0.3
REQ003117076	Calcarenite	Limestone Member	183.19	0.049	0.534	0.020	0.198	-17.0	0.3
REQ003117078	Limestone-shale	Limestone Member	186.63	0.045	0.243	0.022	0.198	-26.6	0.3
REQ003117080	Limestone-shale	Limestone Member	187.48	0.053	0.256	0.022	0.198		
REQ003117084	Limestone-shale	Limestone Member	191.07	0.046	0.628	0.020	0.198	-22.1	0.3
REQ003117086	Limestone-shale	Limestone-shale	193.06	0.037	0.527	0.018	0.198	-17.9	0.3
REQ003117088	Limestone-shale	Limestone Member	193.49	0.036	0.457	0.018	0.198		
REQ003117092	Limestone-shale	Limestone Member	195.96	0.034	0.591	0.018	0.198	-18.7	0.3
REQ003117118	Limestone-shale	Limestone Member	200.47	0.033	0.752	0.018	0.198	-19.0	0.3
REQ003117096	Limestone	Limestone Member	200.66	0.033	0.537	0.025	0.198		
REQ003117104	Shale	Limestone Member	205.42	0.041	0.345	0.029	0.198	-10.2	0.3
3103896_1_3	Limestone-shale	Limestone Member	212.88	0.044	0.213	0.027	0.243	-10.8	0.3
REQ003117116	Calcarenite	Limestone Member	228.13	0.040	0.487	0.045	0.302		

Table S3. references and background information for stratigraphic correlation of S-MIF and S-MDF strata in Fig. 4

Fig 4. Reference	Age (Ma)	Method	Target Sucession	Reference(s)
1	2312.7 ± 5.6	N-TIMS Re-Os	Meteorite Bore member, Turee Creek Group, W. Australia	Philippot et al., 2018
2	2450 ± 3	LA-ICP-MS U-Pb (detrital)	Boolgeeda Iron Formation, Hamersley Group, W. Australia	Caquineau et al., 2018
3	2308 ± 8	SHRIMP U-Pb zircon (volcanic)	Gordon Lake Formation, Huronian Supergroup, N. America	Rasmussen et al., 2013
4	2452.5 ± 6.2	U-Pb zircon (volcanic)	Copper Cliff Rhyolite, Huronian Supergroup, N. America	Ketchum et al., 2013
5	2394 ± 26	Pb-Pb carbonate	Mooidraai Formation , Transvaal Supergroup, S. Africa	Bau et al., 1999
6	2392 ± 23	U-Pb carbonate	Mooidraai Formation , Transvaal Supergroup, S. Africa	Fairey et al., 2013
7	2424 ± 32	ID-TIMS U-Pb baddeleyite (volcanic)	Ongeluk Formation , Transvaal Supergroup, S. Africa	Gumsley et al., 2018
8	2425.5 ± 2.6	ID-TIMS U-Pb baddeleyite (volcanic)	Westerberg Sill Complex , Transvaal Supergroup, S. Africa	Kampmann et al., 2015
9	2415 ± 6	SHRIMP U-Pb zircon (volcanic)	Koegas Subgroup, Transvaal Supergroup, S. Africa	Gutzmer and Beukes, 1998
10	2434 ± 8	SHRIMP U-Pb zircon (volcanic)	Koegas Subgroup, Transvaal Supergroup, S. Africa	Gutzmer and Beukes, 1998; Schier et al., 2018
11	2479 ± 22	ID-NTIMS Re-Os	Koegas Subgroup, Transvaal Supergroup, S. Africa	Kendall et al., 2013
12	2460 ± 5	SHRIMP U-Pb zircon (volcanic)	Asbesheuvals Subgroup, Transvaal Supergroup, S. Africa	Pickard et al., 2003
3	2310 ± 9	SHRIMP U-Pb zircon (volcanic)	Timeball Hill Formation, Transvaal Supergroup, S. Africa	Rasmussen et al., 2013
13	2316 ± 7	Re-Os	Timeball Hill Formation, Transvaal Supergroup, S. Africa	Hannah et al., 2004
14	2480 ± 6		Penge Formation, Transvaal Supergroup, S. Africa	Nelson et al., 1999
15	2434 ± 6.6	ID-TIMS U-Pb zircon (volcanic)	Polisarka Volcanic Formation, NW Russian Federation	Brasier et al., 2013
16	2501.5 ± 1.7	ID-TIMS U-Pb zircon (volcanic)	Pana Tundra Pluton, NW Russian Federation	Amelin et al., 1995

Dataset S1 (separate file): repeat analyses of IAEA-S1 (n=64) between March 2019 and January 2020 giving long-term analytical uncertainty (1σ)

SI References

1. A. Lepland, *et al.*, "5.1 FAR-DEEP Core Archive and Database" in *Reading the Archive of Earth's Oxygenation: Volume 2*, V. A. Melezhik, *et al.*, Eds. (Springer, 2013), pp. 493–502.
2. D. E. Canfield, R. Raiswell, J. T. Westrich, C. M. Reaves, R. A. Berner, The use of chromium reduction in the analysis of reduced inorganic sulfur in sediments and shales. *Chem. Geol.* **54**, 149–155 (1986).
3. G. Izon, *et al.*, Multiple oscillations in Neoarchaean atmospheric chemistry. *Earth Planet. Sci. Lett.* **431**, 264–273 (2015).
4. K. Paiste, *et al.*, Multiple sulphur isotope records tracking basinal and global processes in the 1.98 Ga Zaonega Formation, NW Russia. *Chem. Geol.* **499**, 151–164 (2018).
5. W. U. Ault, M. L. Jensen, Summary of sulfur isotope standards in *Proceedings of the National Science Foundation Symposium at Yale University*, M. L. Jensen, Ed. (1963), pp. 16–29.
6. Y. Ueno, S. Aoyama, Y. Endo, F. Matsu'ura, J. Foriel, Rapid quadruple sulfur isotope analysis at the sub-micromole level by a flash heating with CoF 3. *Chem. Geol.* **419**, 29–35 (2015).
7. J. R. Hulston, H. G. Thode, Variations in the S33, S34, and S36 contents of meteorites and their relation to chemical and nuclear effects. *J. Geophys. Res.* **70**, 3475–3484 (1965).
8. S. Ono, B. Wing, D. Johnston, J. Farquhar, D. Rumble, Mass-dependent fractionation of quadruple stable sulfur isotope system as a new tracer of sulfur biogeochemical cycles. *Geochim. Cosmochim. Acta* **70**, 2238–2252 (2006).
9. D. T. Johnston, J. Farquhar, K. S. Habicht, D. E. Canfield, Sulphur isotopes and the search for life: Strategies for identifying sulphur metabolisms in the rock record and beyond. *Geobiology* **6**, 425–435 (2008).
10. C. Defouilloy, P. Cartigny, N. Assayag, F. Moynier, J. A. Barrat, High-precision sulfur isotope composition of enstatite meteorites and implications of the formation and evolution of their parent bodies. *Geochim. Cosmochim. Acta* **172**, 393–409 (2016).
11. R. J. Carroll, D. Ruppert, The Use and Misuse of Orthogonal Regression in Linear Errors-in-Variables Models. *Am. Stat.* **50**, 1–6 (1996).
12. D. T. Johnston, Multiple sulfur isotopes and the evolution of Earth's surface sulfur cycle. *Earth-Science Rev.* **106**, 161–183 (2011).
13. A. T. Brasier, *et al.*, Earth's earliest global glaciation? Carbonate geochemistry and geochronology of the Polisarka Sedimentary Formation, Kola Peninsula, Russia. *Precambrian Res.* **235**, 278–294 (2013).